Available online at www.sciencedirect.com

ScienceDirect

IFAC PapersOnline CONFERENCE PAPER ARCHIVE

IFAC PapersOnLine 51-20 (2018) 222–227

Flatness-based hierarchical control of a meshed DC microgrid

I. Zafeiratou * **D. V. A. Nguyen** * **I. Prodan** * **L. Lefèvre** * **L. Piétrac** **

* *Univ. Grenoble Alpes, Grenoble INP ⋆, LCIS, F-26000 Valence, France (e-mail: igyso.zafeiratou, dang − viet − anh.nguyen, ionela.prodan, laurent.lefevre@lcis.grenoble-inp.fr)*

** *Université de Lyon, CNRS, INSA-Lyon, AMPERE, F-69621 Villeurbanne, France (e-mail: laurent.pietrac@insa-lyon.fr)*

Abstract: This paper proposes a meshed DC microgrid architecture supervised by a multi-layer optimization based control. Its dynamical analysis is described through the Bond Graph notion and the port-Hamiltonian formalism. A multiscale supervision scheduling is developed to handle the load balancing problem for the proper energy distribution within the transmission network. The control architecture considers three control layers. These are implemented via a combination of differential flatness and MPC (Model Predictive Conctrol).

Keywords: Meshed DC microgrid, Port-Hamiltonian formalism, Differential flatness, B-splines parametrization, Power balancing, Model Predictive Control

1. INTRODUCTION

Recently, the increasing demand on energy consumption in buildings (residential, commercial, industrial) requires flexibility and efficiency on energy generation. Although the traditional grid is generally useful for the energy production, some disadvantages appear. The main grid cannot offer energy independence and does not ensure the continuity of the power transmission. As a consequence the interest on microgrids has increased due to their high reliability when different distributed energy ressources (DERs) are integrated into a power system.

The following work presents a DC microgrid architecture, as shown in Fig. 1 with a meshed topology, which signifies that the power is generated by a collection of DERs (utility grid-UG, solar panel-PV, storage facility-ES) and passes through multiple possible paths until it reaches its final point. Consequently, a possible interruption of the power transmission can be avoided and the constant and safe operation of the system can be ensured. The aforementioned components in combination with their topology result in a strongly nonlinear system, distributed in space and in time. The global system dynamics is separated into different timescales. Primarily, the existence of the DC/DC converters useful for the voltage regulation to and from the common DC-bus creates a fast dynamics. Secondly, the slow dynamics is related to the ES and the PV system operation. At the same time, we have to cope with variable profiles and costs and obey to a set of constraints related to the different characteristics of the system components.

The microgrid energy management problem is generally formulated as a constrained optimization problem in continuous time, not straightforward to solve. In the literature, there are several methods proposed for the modeling and control of such systems. Because of their complexity, most of the times, they propose a simple dynamics in order to proceed to its supervision. Furthermore, there are researchers that look into multi-layer approaches where the generated profiles may not fully respect the constraints or the dynamics of the system. Various works concentrate on the use of MPC in combination with mixed-integer programming for battery scheduling or chance constraints to deal with profiles uncertainties (Velarde et al., 2017). The hierarchical implementation of MPC is discussed in (Parisio et al., 2014) for microgrids operating in islanded mode. A two-layer control and coordination for DERs is addressed in (Drgoňa et al., 2018) through the use of MPC via machine learning.

This paper builds upon our previous results where a port-Hamiltonian (PH) model was developed for each component of the DC microgrid. In here, we go further in i) developing a flat representation of the strongly nonlinear interconnected system and ii) dealing with the optimization-based control of the global meshed DC microgrid.

2. DC MICROGRID MODEL

In this section, we recall briefly the dynamical model of the system which was developped using a Bond Graph represenatation and a PH (Port-Hamiltonian) formalism. A detailed presentation of the model is given in Zafeiratou et al. (2018). Next, we derive its flat representation and present the advantages of the associated B-splines parametrization.

2.1 Dynamical representation of the microgrid model

The system presented in Fig.1 is further represented as a set of electrical RLC circuits as shown in Fig. 2. Its

⋆ Institute of Engineering Univ. Grenoble Alpes

2405-8963 © 2018, IFAC (International Federation of Automatic Control) Hosting by Elsevier Ltd. All rights reserved.
Peer review under responsibility of International Federation of Automatic Control.
10.1016/j.ifacol.2018.11.017

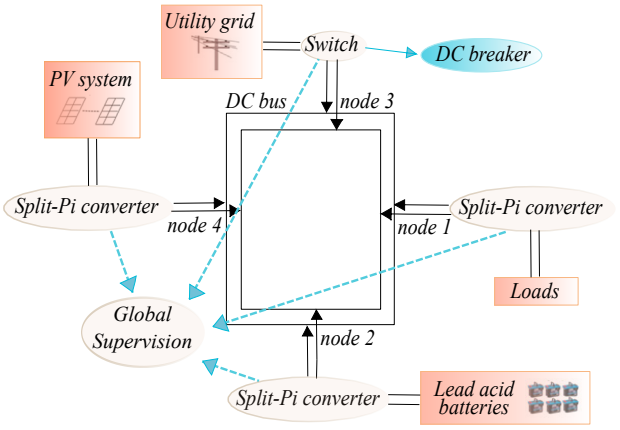

Fig. 1. Meshed DC microgrid architecture.

main components, for which we provide below their mathematical representation, are the Split-Pi converter and the ES system considered here as a lead acid battery described by the Kinetic Battery Model (KiBaM) (Fig. 2). We provide profiles generated from the PV model proposed in Zafeiratou et al. (2018) as well as for the load demand.

Split-Pi converter: The PH model of the Split-Pi converter is obtained from its Bond Graph representation (Zafeiratou et al., 2018) as follows:

$$\begin{cases} \begin{bmatrix} \dot{p}_{1sc}(t) \\ \dot{p}_{2sc}(t) \\ \dot{q}_{1sc}(t) \\ \dot{q}_{2sc}(t) \\ \dot{q}_{3sc}(t) \end{bmatrix} = [J_{sc}(t) - R_{sc}]Q_{sc}x_{sc}(t) + \begin{bmatrix} 0 & 0 \\ 0 & 0 \\ \frac{-1}{R_{1sc}} & 0 \\ 0 & 0 \\ 0 & 1 \end{bmatrix} u_{sc}(t), \\ i_{DC}(t) = \begin{bmatrix} 0 & 0 & \frac{-1}{R_{1sc}} & 0 & 0 \\ 0 & 0 & 0 & 0 & 1 \end{bmatrix} Q_{sc}x_{sc}(t) - \begin{bmatrix} \frac{1}{R_{1sc}} & 0 \\ 0 & 0 \end{bmatrix} u_{sc}(t), \end{cases} \tag{1}$$

where $x_{sc}(t) = [p_{1sc}(t)\ p_{2sc}(t)\ q_{1sc}(t)\ q_{2sc}(t)\ q_{3sc}(t)]^\top \in \mathbb{R}^5$ is the state vector, where p is the magnetic flux of the corresponding inductors and q is the charge of the corresponding capacitors, $u_{DC}(t) = [-v_{DC}(t)\ -i_{R_{Lsc}}(t)]^\top \in \mathbb{R}^2$ is the input vector represented by the input voltage, $v_{DC}(t)$, coming from the common DC-bus, and the load current $i_{R_{Lsc}}(t) = \frac{q_{3sc}(t)}{R_{Lsc}C_{3sc}}$. Also, in (1) $y_{sc}(t) = [i_{DC}(t)\ v_{R_{Lsc}}(t)]^\top \in \mathbb{R}^2$ is the output vector, $i_{DC}(t) \in \mathbb{R}$ is the current of the DC-bus and $v_{R_{Lsc}(t)\in\mathbb{R}}$ is the output voltage of the converter. The matrix Q_{sc} is the circuit's parameter matrix equal to $diag(1/I_{1sc},\ 1/I_{1sc},\ 1/C_{1sc},\ 1/C_{2sc},\ 1/C_{3sc}) \in \mathbb{R}^{5\times5}$, where C is the capacitance of the corresponding capacitors and I is the inductance of the corresponding inductors. The matrix $J_{sc}(t) \in \mathbb{R}^{5\times5}$ and the dissipation matrix $R_{sc} \in \mathbb{R}^{5\times5}$ are described below:

$$J_{sc}(t) = \begin{bmatrix} 0 & 0 & 1 & -(1-d_{1sc}(t)) & 0 \\ 0 & 0 & 0 & (1-d_{2sc}(t)) & -1 \\ -1 & 0 & 0 & 0 & 0 \\ 1-d_{1sc}(t) & -(1-d_{2sc}(t)) & 0 & 0 & 0 \\ 0 & 1 & 0 & 0 & 0 \end{bmatrix}, \tag{2}$$

$$R_{sc} = diag(0,\ 0,\ \frac{1}{R_{1_{sc}}},\ 0,\ 0), \tag{3}$$

with $d_{1sc}(t), d_{2sc}(t) \in [0,1]$, the duty cycles. Hence, the Split-Pi converter in (1) is a non-linear model.

Lead-acid battery: Here, we use the two tank Kinetic Battery Model (KiBaM). As represented in Fig. 2, the RLC circuit of the lead acid battery is composed by two capacitors C_{1b} and C_{2b} separated by a resistor R_{2b}. Similarly, the PH model of the KiBaM is obtained from its Bond Graph representation as follows:

$$\begin{cases} \begin{bmatrix} \dot{q}_{1b}(t) \\ \dot{q}_{2b}(t) \end{bmatrix} = [J_b(t) - R_b]Q_b x_b(t) + \begin{bmatrix} \frac{1}{R_{1b}} \\ 0 \end{bmatrix} (v_{sc}(t)), \\ i_{sc}(t) = \begin{bmatrix} -\frac{1}{R_{1b}} & 0 \end{bmatrix} Q_b x_b(t) + \begin{bmatrix} \frac{1}{R_{1b}} \end{bmatrix} v_{sc}(t), \end{cases} \tag{4}$$

where $x_b = [q_{1b}(t)\ q_{2b}(t)]^\top \in \mathbb{R}^2$ is the state vector, where q is the charge of the capacitors, $v_{sc}(t) \in \mathbb{R}$ is the system's input vector denoting the input voltage coming from the Split-Pi converter connected with the battery, $i_{sc}(t) \in \mathbb{R}$ is the output vector, where $i_{sc}(t)$ indicates the battery current during charging. The circuit's parameter matrix is given by $Q_b = diag(1/C_{1b},\ 1/C_{2b}) \in \mathbb{R}^{2\times2}$. The dissipation matrix $R_b \in \mathbb{R}^{2\times2}$ is:

$$R_b = \begin{bmatrix} \frac{1}{R_{1b}} + \frac{1}{R_{2b}} & -\frac{1}{R_{2b}} \\ -\frac{1}{R_{2b}} & \frac{1}{R_{2b}} \end{bmatrix}. \tag{5}$$

The matrix $J_b(t)$ in (4) is equal to 0, thus we conclude in a linear model for the battery.

Central transmission line network: The mathematical analysis of the central transmission network is based on its Bond Graph and on the power conservation principle as presented below:

$$P_{ug}(t)+P_{pv}(t) - P_{es}(t) - P_{loads}(t) - P_{R1b}(t) - P_{R1}(t)- \\ -P_{R2}(t) - P_{R3}(t) - P_{R4}(t) - 3P_{R_{1sc}}(t) = 0, \tag{6}$$

where $P(t)$ is the power of each corresponding element.

2.2 Flat representation of the DC microgrid

In this section, the state-space representation of the battery (4) connected to the Split-Pi converter (1) will be replaced by the flatness-based representation of the interconnected system. This will be used next for the optimal reference profiles generation in the high level.

In general, the set of flat outputs of a nonlinear system is not straightforward to find, as also shown by the complex dynamical equations of the Split-Pi and battery given in (1) and (4). Luckily, existing results from literature provide hints towards constructive approaches (Levine, 2009; Franke and Robenack, 2013). In order to proceed to the flat output calculation, we consider the following: i) in (1) and (4) the system is described by 7 states; $p_{1sc}(t)$, $p_{2sc}(t)$, $q_{1sc}(t)$, $q_{2sc}(t)$, $q_{3sc}(t)$, $q_{1b}(t)$, $q_{2b}(t)$, ii) in (1) and (4) we have 4 inputs in our system: $d_{1sc}(t)$, $d_{2sc}(t)$, $V_{sc}(t)$, $I_{R_{1b}}(t)$, leading to a set of four flat outputs, iii) the circuit's parameters and the values of the resistors are constants.

Proposition 1: The dynamical PH model given in (1), (2), (4) and (5) is differentially flat corresponding to the following set of flat outputs:

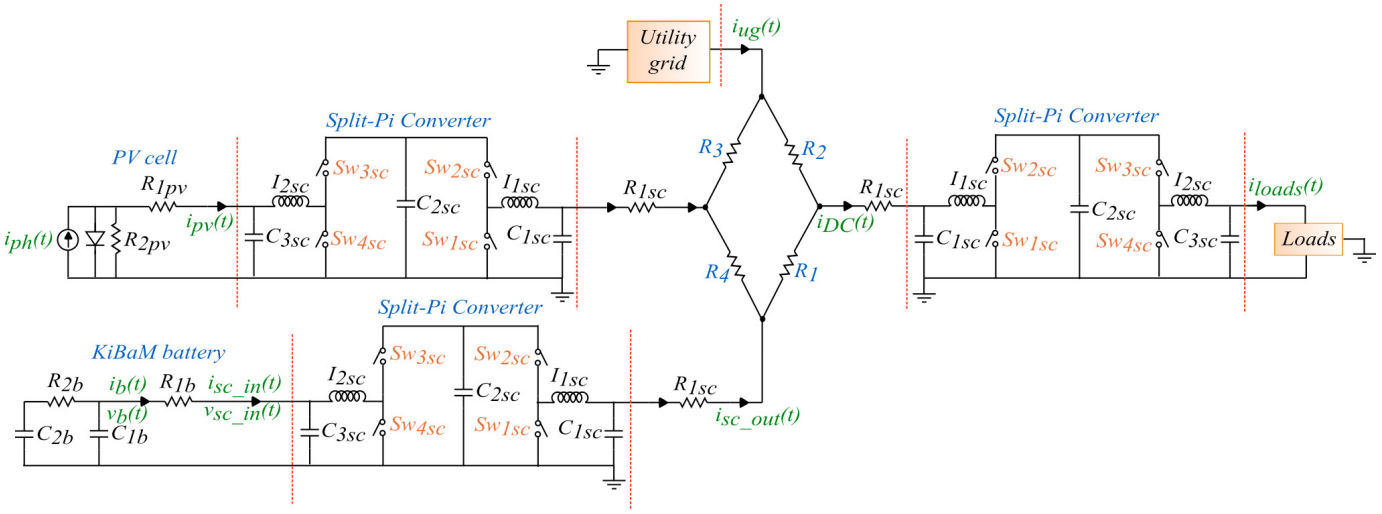

Fig. 2. RLC circuit representation of the DC microgrid.

$$
\begin{aligned}
z_1(t) &= \frac{1}{I_{1sc}}\frac{p_{1sc}(t)^2}{2} + \frac{1}{I_{2sc}}\frac{p_{2sc}(t)^2}{2} + \frac{1}{C_{2sc}}\frac{q_{2sc}(t)^2}{2},\\
z_2(t) &= q_{3sc}(t) + q_{1b}(t),\\
z_3(t) &= q_{2b}(t),\\
z_4(t) &= q_{2sc}(t).
\end{aligned} \tag{7}
$$

Proof: The system mentioned in (1), (2), (4) and (5) is flat since the output vector can be expressed in function of the states, their derivatives and the inputs and vice versa. Additionally to this, the matrices $G_{sc}(t) \in \mathbb{R}^{5\times 2}$ and $G_b(t) \in \mathbb{R}^2$ in the PH representations are constant and invertible. The total energy $H(x)$ is given in quadratic form, since the circuit's parameter matrices $Q_{sc} \in \mathbb{R}^{5\times 5}$ and $Q_b \in \mathbb{R}^{2\times 2}$ are constant. Consequently, from the definition of differential flatness (Levine, 2009), we can easily infer that the system is controllable and flat. □

Concerning the method of parametrization, we chose to use B-splines due to their advantageous properties on convexity and on calculating the flat outputs' derivatives. Their degree depends on the highest order derivative to which the continuity needs to be ensured. Generally, we consider that the flat output $z(t)$ is projected over N B-splines of order d as in the following (Suryawan, 2012):

$$z(t) = \sum_{i=1}^{N} p_i \cdot b_{i,d}(t) = \mathcal{P}\mathcal{B}_d(t), \tag{8}$$

where $p_i \in \mathbb{R}^3$ is the i^{th} control point, to which it corresponds the matrix $\mathcal{P} \in \mathbb{R}^{3\times N}$ of N control points equal to $\mathcal{P} = [p_1\ p_2\ ...\ p_N]^\top$. Moreover, $\mathcal{B}_d(t) = [b_{1,d}(t)\ b_{2,d}(t)\ ...\ b_{N,d}(t)]^\top$ is the B-spline vector, where $b_{i,d}(t)$ corresponds to the i^{th} b-spline of order d. The b-splines are defined by a knot-vector $T \in \mathbb{R}^{N+d}$ which is a set of non-decreasing time instants equal to $T = \{\tau_0 \leq \tau_1 \leq ... \leq \tau_m\}$, where $m = N + d + 1$.

3. MULTI-LAYER OPTIMIZATION

The main goal is to minimize the electricity cost by minimizing the energy consumption from the UG, hence taking advantage of the PV power production and the ES system capacity. The control variables within the DC microgrid system are: the duty cycles $d_{1sc}(t)$, $d_{2sc}(t)$ in (2) of the Split-Pi converter and the UG power $P_{ug}(t)$. Gathering all the elements, presented in section 2, we present hereinafter the control approach (illustrated in Fig.3) that we propose:

- at the *high level* we use the flat representation of the Split-Pi converter and the battery system and generate optimal reference profiles for the battery current and voltage, denoted as i_b and v_b respectively. At the same time, we take into account the system dynamics and the continuous-time constraints validation.
- at the *middle level* we use the a priori given profiles and track them in a constrained MPC framework.
- at the *low level* we control the duty cycles of the DC/DC converters, considering the tracking profiles obtained from the MPC controller in the middle level.

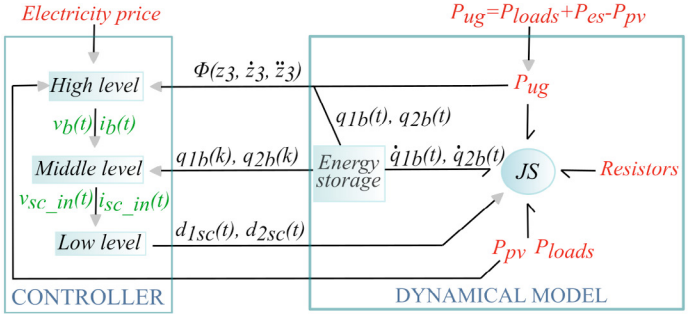

Fig. 3. Hierarchical control scheme of the DC microgrid.

We will concentrate next only on the high and middle level of the hierarchical control scheme. Note that we do not consider the power losses of the system. Therefore, the power balancing equation (6) becomes:

$$P_{ug} + P_{pv} - P_{es} - P_{loads} = 0, \tag{9}$$

where the resistances' power sets to zero, $P_{R1} = P_{R2} = P_{R3} = P_{R4} = P_{R_{1sc}} = P_{R_{1b}} = 0$.

3.1 High level: optimal profiles generation through flatness

The general objective of the high level problem is to generate appropriate profiles related to the battery charges and discharges while minimizing the electricity purchase

from the UG. Hence, the following cost function needs to be minimized in the presence of constraints:

$$\mathcal{J}_h = \int_{t_0}^{t_f} e(t)P_{ug}(t)dt, \tag{10}$$

$$\begin{aligned} subject\ to:\ & system\ dynamics\ (1)-(7),\\ & v_{b\_minh} \le v_b(t) \le v_{b\_maxh}, && (11)\\ & i_{b\_minh} \le i_b(t) \le i_{b\_maxh}, && (12)\\ & q_{2b\_minh} \le q_{2b}(t) \le q_{2b\_maxh}, && (13)\\ & P_{ug\_minh} \le P_{ug}(t) \le P_{ug\_maxh}, && (14) \end{aligned}$$

where $e(t)$ is the electricity price.

In order to proceed to the optimal solution of our problem, firstly we derive from the power conservation equation (9) that $P_{ug}(t) = P_{es}(t) + P_{loads}(t) - P_{pv}(t)$. Then, we obtain a relation between the $P_{ug}(t)$ and the battery current and voltage. Considering the q_{1b} and $i_{R_{1b}}(t)$ in function of the flat outputs in (7), the $i_b(t)$ and $v_b(t)$, which contain also the references to be followed, can be particularly expressed as follows:

$$i_b(t) = C_{1b}R_{2b}\ddot{z}_3(t) + (\frac{C_{1b}}{C_{2b}} + 1)\dot{z}_3(t), \tag{15}$$

$$v_b(t) = R_{2b}\dot{z}_3(t) + \frac{1}{C_{2b}}z_3(t). \tag{16}$$

The obtained profiles need to respect continuous-time constraints. If these are validated all the time, it will be easier for the middle level controller to follow them.

Since (15) and (16) depend on the flat output $z_3(t)$ we proceed next to the parametrization of $z_3(t)$ by using B-splines basis functions as in (Suryawan, 2012).

Therefore, we describe the B-splines as it follows:

$$\mathcal{B}_d^{(r)}(t) = M_{d,d-r}\mathcal{B}_{d-r}(t) = M_{d,d-r}S_{k,d-r,d}\mathcal{B}_d(t), \quad \forall t \in [\tau_k, \tau_{k+1}). \tag{17}$$

From (15), (16) and (17), we obtain the following for the battery's output current and voltage:

$$\begin{aligned} v_b(t) &= \sum_{i=1}^{N}\left[\frac{1}{C_{2b}}p_i + R_{2b}\left(\mathcal{P}M_{d,d-1}S_{k,d-1,d}\right)_i\right]\mathcal{B}_{i,d}(t),\\ i_b(t) &= \sum_{i=1}^{N}\left[\left(1+\frac{C_{1b}}{C_{2b}}\right)\left(\mathcal{P}M_{d,d-1}S_{k,d-1,d}\right)_i + C_{1b}R_{2b}\cdot\right.\\ &\quad \left.\cdot\left(\mathcal{P}M_{d,d-2}S_{k,d-2,d}\right)_i\right]\mathcal{B}_{i,d}(t),\ \ \forall t \in [\tau_k, \tau_{k+1}). \end{aligned} \tag{18}$$

Using the above relations we rewrite the cost function in (10) as:

$$\begin{aligned} \mathcal{J}_h &= \int_{t_0}^{t_f} e(t)(P_{es}(t) + P_{loads}(t) - P_{pv}(t))dt = \\ &= \int_{t_0}^{t_f} e(t)(i_b(t)v_b(t) + P_{loads}(t) - P_{pv}(t))dt. \end{aligned} \tag{19}$$

which is introduced in the following optimization problem corresponding to (10)-(14):

$$\min_{i_b(t)v_b(t)} \int_{t_0}^{t_f} e(t)(i_b(t)v_b(t) + P_{loads}(t) - P_{pv}(t))dt \tag{20}$$

$$subject\ to: v_{b\_minh} \le p_{k_i}^{v_b}\mathcal{B}_{i,d}(t) \le v_{b\_maxh}, \tag{21}$$

$$i_{b\_minh} \le \sum_{i=1}^{N} p_{k_i}^{i_b}\mathcal{B}_{i,d}(t) \le i_{b\_maxh}, \tag{22}$$

$$q_{2b\_minh} \le \sum_{i=1}^{N} p_i\mathcal{B}_{i,d}(t) \le q_{2b\_maxh}, \tag{23}$$

$$P_{ug\_minh} \le P_{ug} \le P_{ug\_maxh}, \tag{24}$$

Concerning the constraints, for (21) and (22) we have:

$$\begin{aligned} p_{k_i}^{v_b} &= \frac{1}{C_{2b}}p_i + R_{2b}\left(\mathcal{P}M_{d,d-1}S_{k,d-1,d}\right)_i,\\ p_{k_i}^{i_b} &= \left(1+\frac{C_{1b}}{C_{2b}}\right)\left(\mathcal{P}M_{d,d-1}S_{k,d-1,d}\right)_i + C_{1b}R_{2b}\cdot\\ &\quad\cdot\left(\mathcal{P}M_{d,d-2}S_{k,d-2,d}\right)_i, \end{aligned}$$

derived from (18). For the P_{ug} constraint in (24), we use the power conservation equation of (9) as shown below:

$$P_{ug\_minh} - P_{loads} + P_{pv} \le P_{es} \le P_{ug\_maxh} - P_{loads} + P_{pv}. \tag{25}$$

The reference profiles obtained here for the battery current and voltage will be denoted in the middle level as i_b^{ref} and v_b^{ref} correspondingly. The detailed calculation of the cost function in (19) is given in Appendix A.

3.2 Middle level control problem formulation

In this subsection, we consider an MPC based controller for tracking the Split-Pi converter output voltage v_{sc_in}. Firstly, we need to obtain its reference profile. Considering the Ohm's law $\Delta v = i \cdot R$, we take into account the following relation:

$$v_{sc\_in}^{ref}(t) = v_b^{ref}(t) + i_b^{ref}(t)R_{1b}. \tag{26}$$

Afterwards, we proceed to the system discretization. Firstly, we consider the state vector $\tilde{x}(t)$ given as $\tilde{x}(t) = [q_{1b}(t)\ q_{2b}(t)]^\top$, the input $\tilde{u}(t) \in \mathbb{R}$ as $\tilde{u}(t) = v_{sc\_in}(t)$ and the output vector $\tilde{y}(t) \in \mathbb{R}^2$ as $\tilde{y}(t) = [i_b(t)\ v_b(t)]^\top$, where $i_b(t) = i_{sc}(t)$ and $v_b(t) = \frac{q_{1b}(t)}{C_{1b}}$. We result in a continuous-time SIMO (single input multiple output) problem. The solution will be given through Euler explicit. Hence we result in the following discretized system:

$$\begin{cases} \tilde{x}(k+1) &= A\tilde{x}(k) + B\tilde{u}(k),\\ \tilde{y}(k) &= C\tilde{x}(k) + D\tilde{u}(k), \end{cases} \tag{27}$$

where matrices $A \in \mathbb{R}^{2\times2}$, $B \in \mathbb{R}^2$, $C \in \mathbb{R}^{2\times2}$ and $D \in \mathbb{R}^2$ are equal to:

$$A = \begin{bmatrix} 1 - \frac{T_s}{C_{1b}}\left(\frac{1}{R_{1b}} + \frac{1}{R_{2b}}\right) & \frac{T_s}{C_{2b}R_{2b}} \\ \frac{T_s}{C_{1b}R_{2b}} & 1 - \frac{T_s}{C_{2b}R_{2b}} \end{bmatrix},\ B = \begin{bmatrix} \frac{T_s}{R_{1b}} \\ 0 \end{bmatrix},$$

$$C = \begin{bmatrix} -\frac{1}{C_{1b}R_{1b}} & 0 \\ \frac{1}{C_{1b}} & 0 \end{bmatrix},\ D = \begin{bmatrix} \frac{1}{R_{1b}} \\ 0 \end{bmatrix},$$

Therefore, we continue with the MPC controller design that will track the i_b, v_b and v_{sc_in}, considering the generated optimal profiles obtained in the high level as references. We consider an objective function and we solve the following optimization problem over a receding prediction horizon N_p:

$$\min_{\tilde{u}(k)} \sum_{i=k}^{k+N_p-1} (\tilde{y}(i) - \tilde{y}^{ref}(i))^\top Q_{\tilde{y}}(\tilde{y}(i) - \tilde{y}^{ref}(i)) + \tag{28}$$

$$+(\tilde{u}(i) - \tilde{u}^{ref}(i))^\top R_{\tilde{u}}\left(\tilde{u}(i) - \tilde{u}^{ref}(i)\right) \tag{29}$$

$$subject\ \ to: v_{b\_minm} \leq v_b(t) \leq v_{b\_maxm}, \quad (30)$$
$$i_{b\_minm} \leq i_b(t) \leq i_{b\_maxm}, \quad (31)$$
$$q_{2b\_minm} \leq q_{2b}(t) \leq q_{2b\_maxm}, \quad (32)$$
$$P_{ug\_minm} \leq P_{ug}(t) \leq P_{ug\_maxm} \quad (33)$$
$$and\ to:\ the\ system\ (27). \quad (34)$$

At this point, we mention that we deal with an objective function in quadratic form with nonlinear constraints and with a variable electricity cost.

4. SIMULATION RESULTS

In this section, we present the simulation results of the high and the middle level that have been previously presented. Table 1 and 2 delineate the DC microgrid model parameters and the simulation settings.

Table 1. Model parameters for the simulations.

Variable	Units	Values
$R_{1sc},\ R_{1b},\ R_{2b}$	$[\Omega]$	0.1, 0.025, 11.34
$I_{1sc},\ I_{2sc}$	$[H]$	0.25, 0.25
$C_{1sc},\ C_{2sc},\ C_{3sc}$	$[F]$	0.0008, 0.0008, 0.0008
$C_{1b},\ C_{2b}$	$[F]$	86400, 21600

Table 2. System settings for the simulations.

Levels	Variable	Values
High level	N as in (17)	20
	d as in (17)	4
Constraints parameters	$v_{b\_minh},\ v_{b\_maxh}$	12.1, 12.9 $[V]$
	$i_{b\_minh},\ i_{b\_maxh}$	$-14.5,\ 19.5$ $[A]$
	$q_{2b\_minh},\ q_{2b\_maxh}$	72.6, 77.4 $[Ah]$
	$P_{ug\_minh},\ P_{ug\_maxh}$	$-2000,\ 4100$ $[W]$
Middle level	N_p as in (28)	10
	T_s as in (28)	60 $[s]$
	Q_y as in (28)	$diag(1,1)$
	R_u as in (28)	800
Constraints parameters	$v_{b\_minm},\ v_{b\_maxm}$	12, 13 $[V]$
	$i_{b\_minm},\ i_{b\_maxm}$	$-15,\ 20$ $[A]$
	$q_{2b\_minm},\ q_{2b\_maxm}$	72, 78 $[Ah]$
	P_{ug_minm}, P_{ug_maxm}	$-2100,\ 4200$ $[W]$

For the simulation we used a set of DS-100 PV modules by collecting real external temperature and irradiation data of a whole day in June. Concerning the battery unit, we considered a collection of AGM 12-165 model of lead acid batteries. For the electricity price, we kept a variable cost equal to 0.147 $[eur/kWh]$ from 4:00pm until 10:00pm and equal to 0.116 $[eur/kWh]$ for the rest of the day. For the simulations acquisition we use MATLAB 2015a. Additionally, we choose the YALMIP solver for both the high and the middle level.

In order to carry on with the simulations on the high level and be able to use them as reference profiles in the middle level control, we should appear more restricted constraints as it appears in Table 2. Solving the optimization problem expressed in function of the control points and B-splines (20) we obtain the reference profiles for the battery charge and discharge as well as the current and voltage as given in Fig.4. Furthermore, Fig.5 illustrates the power generated from the battery and the utility grid within 24 hours with the PV and the loads demand profiles. We mention here that the power's positive sign indicates the power

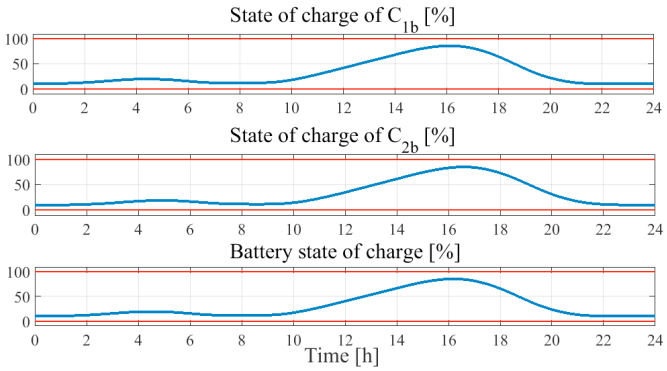

Fig. 4. Optimal trajectories of the battery state of charge.

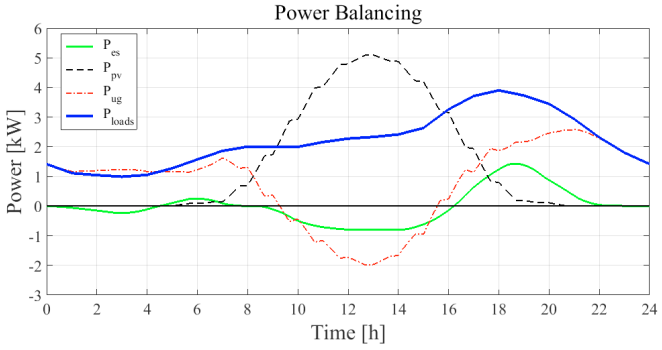

Fig. 5. Power balancing optimal reference profiles.

Table 3. Simulation results of different N.

N	20	25	30	35	40
d	4	4	4	4	4
Electricity cost [euros]	2.514	2.427	2.448	2.396	2.125
Calculation time [s]	134	197	309	444	535
Number of charge/discharge	4	6	5	9	11

supplied to the microgrid. Moreover, we notice that in case of PV power excess, this amount of power does not get wasted. It is either sold to the UG or charges the ES system. In addition, after 5:00pm when the load demand starts to increase, both the battery and the external grid try to support the consumer's demand. Table 3 shows the electricity cost, the calculation time and the number of charges and discharges of the battery for several control points, N, in the B-splines parametrization. We observe that as the number of control points increases the electricity cost decreases, while the battery charges and discharges get increased. The electricity cost without using the battery is equal to 2.818 $euros$.

Next, we present the results that concern the middle level control. Disturbances were considered in the control input that represents the input voltage of the Split-Pi converter, v_{sc_in}. The disturbance magnitude used for the simulations is about 5% of the difference between the minimum and the maximum value of the $v_{sc\_in}^{ref}$. In Fig. 6 and Fig.7, we see that the trajectories are well followed and satisfied.

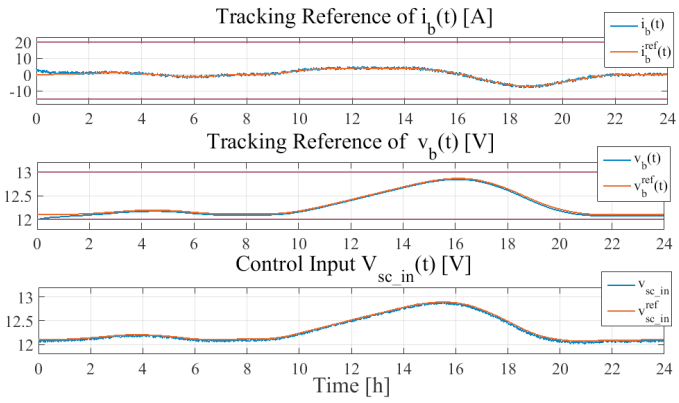

Fig. 6. Battery trajectory tracking under perturbation.

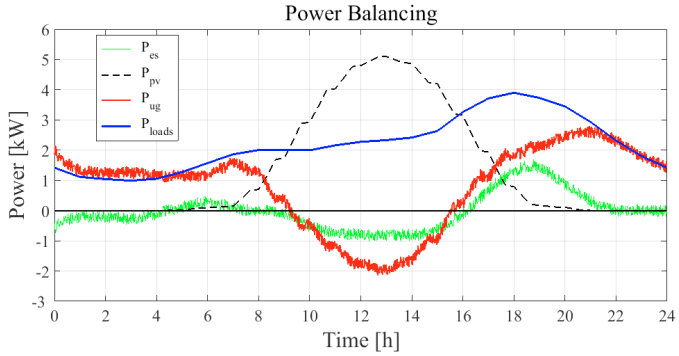

Fig. 7. Tracking profiles under perturbation.

5. CONCLUSION

In this paper, we have introduced a multi-layer supervision for a meshed DC microgrid. We presented a constrained optimization control approach for the power balancing problem formulation at the high and the middle level and we provided the corresponding simulation results. In a meshed topology, the optimization problem to solve becomes more complicated since it contains a combination of sources. The controller takes decisions for the power supply of loads according the less costly DER that exists in the system, in our case the PV and the ES systems. Henceforward, we intend for further improvements in our optimization constrained-based problem formulation by taking into account the power losses within the DC-bus. Furthermore, we plan to employ the obtained optimal profiles of the middle level to the low level control for the switching activity acquisition.

ACKNOWLEDGEMENTS

This work is funded by the French National Research Agency within the framework of the project ANR-15-CE05-004-02 $C^3\mu$ (Components, Control and Communication).

REFERENCES

Drgoňa, J., Picard, D., Kvasnica, M., and Helsen, L. (2018). Approximate model predictive building control via machine learning. *Applied Energy*, 218, 199–216.

Franke, M. and Robenack, K. (2013). On the computation of flat outputs for nonlinear control systems. In *Control Conference (ECC), 2013 European*, 167–172. IEEE.

Levine, J. (2009). *Analysis and control of nonlinear systems: A flatness-based approach*. Springer Science & Business Media.

Parisio, A., Rikos, E., and Glielmo, L. (2014). A model predictive control approach to microgrid operation optimization. *IEEE Transactions on Control Systems Technology*, 22(5), 1813–1827.

Stoican, F., Prodan, I., Popescu, D., and Ichim, L. (2017). Constrained trajectory generation for uav systems using a b-spline parametrization. In *Control and Automation (MED), 2017 25th Mediterranean Conference on*, 613–618. IEEE.

Suryawan, F. (2012). *Constrained Trajectory Generation and Fault Tolerant Control Based on Differential Flatness and B-splines*. Ph.D. thesis, School of Electrical Engineering and Computer Science, The University of Newcastle, Australia.

Velarde, P., Valverde, L., Maestre, J., Ocampo-Martinez, C., and Bordons, C. (2017). On the comparison of stochastic model predictive control strategies applied to a hydrogen-based microgrid. *Journal of Power Sources*, 343, 161–173.

Zafeiratou, I., Prodan, I., Lefèvre, L., and Piétrac, L. (2018). Dynamical modelling of a dc microgrid using a port-hamiltonian formalism. *9th Vienna International Conference on Mathematical Modelling, IFAC*.

Appendix A. EXPLICIT CALCULATION OF THE OBJECTIVE FUNCTION

In this appendix, we proceed to the detailed calculations of the objective function in (28) as following:

$$\mathcal{J} = \int_{t_0}^{t_f} e(t)[P_{loads}(t) - P_{pv}(t)]\mathrm{d}t + \int_{t_0}^{t_f} e(t) i_b(t) v_b(t) \mathrm{d}t = $$
$$= \mathcal{J}_p + \mathcal{J}_b.$$

We obtain the following (Stoican et al., 2017):

$$\mathcal{J}_b = \int_{t_0}^{t_f} e(t) \left[\frac{1}{C_{2b}} \left(\sum_{i=1}^{N} p_i \mathcal{B}_{i,d}(t) \right) + R_{2b} \left(\sum_{i=1}^{N} p_i M_{d,d-1} \cdot \right.\right.$$
$$\left.\cdot \mathcal{B}_{i,d-1}(t) \right] \left[\left(\frac{C_{1b}}{C_{2b}} + 1 \right) \left(\sum_{i=1}^{N} p_i M_{d,d-1} \mathcal{B}_{i,d-1}(t) \right) + \right.$$
$$\left. + C_{1b} R_{2b} \left(\sum_{i=1}^{N} p_i . M_{d,d-2} . \mathcal{B}_{i,d-2}(t) \right) \right] \mathrm{d}t =>$$
$$=> \mathcal{J} = Term_1 + Term_2 + Term_3 + Term_4, \ where,$$
$$Term_1 = f \left(\frac{C_{1b}}{C_{2b}} + 1 \right) \int_{t_0}^{t_f} e(t) \left(\sum_{i=1}^{N} p_i \mathcal{B}_{i,d}(t) \right)^T \cdot$$
$$\cdot \left(\sum_{j=1}^{N} \left(\mathcal{P} M_{d,d-1} \right)_j \mathcal{B}_{j,d-1}(t) \right) \mathrm{d}t$$

Since the integral in the previous expression of $Term_1$ results in scalar values, we obtain the cost function in quadratic form. Similarly, we proceed to the calculation of the other terms.